Lessons Learned from the BEAVRS Benchmark

Benoit Forget
Massachusetts Institute of Technology
October 12, 2022

BEAVRS Benchmark

- What is it?
  - The BEAVRS benchmark is a 4-loop PWR description of an operating US reactor which provides measurement data for the first 2 cycles of operation.
- Why we did it?
  - As part of work at MIT on the development of high-fidelity simulation tools for full core reactor analysis, there was growing concern that the community lacked a proper benchmark to truly test and validate these methods.
    - Real assembly design
    - Real enrichment data
    - Real power distribution
    - Real core shuffling pattern
    - Real burnable poison distribution
    - …

N. HORELIK, B. HERMAN, B. FORGET, K. SMITH, "Benchmark for Evaluation and Validation of Reactor Simulations (BEAVRS)", Proc. M&C 2013, Sun Valley, Idaho, May 5-9, 2013.

Description

- 193 fuel assemblies
  - 8 grid spacers
    - Different top/bottom and intermediate spacers
    - No design provided but weight known
  - Pyrex burnable absorbers
    - Asymmetric pattern
  - Exact as-built enrichment known for each individual fuel location

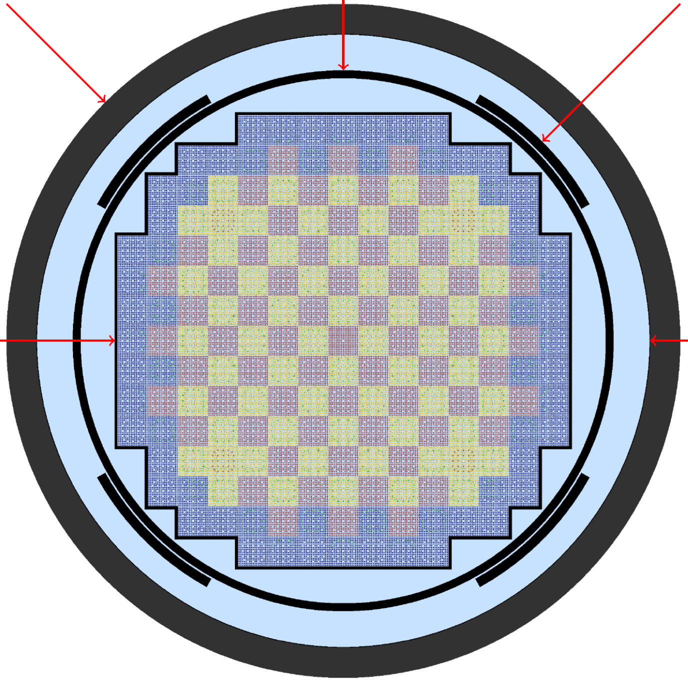

Table 1: Summary of key model parameters.

Core Lattice		Source
No. Fuel Assemblies	193	1
Loading Pattern	w/o U235	
Region 1 (cycle 1)	1.60†	1
Region 2 (cycle 1)	2.40†	1
Region 3 (cycle 1)	3.10†	1
Region 4A (cycle 2)	3.20††	1
Region 4B (cycle 2)	3.40††	1
Cycle 1 Heavy Metal Loading	81.8 MT	3
Fuel Assemblies		
Pin Lattice Configuration	17 × 17	4
Active Fuel Length	365.76 cm	5
No. Fuel Rods	264	4
No. Grid Spacers	8	4
Control		
Control Rod Material (Upper Region)	B4C	57
Control Rod Material (Lower Region)	Ag-In-Cd	56
No. Control Rod Banks	57	1
No. Burnable Poison Rods in Core	1266	1
Burnable Poison Material	Borosilicate Glass, 12.5 w/o B_2O_3	4
Performance		
Core Power	3411 MWth	6
Operating Pressure	2250 psia	6
Core Flow Rate	61.5×10^6 kg/hr (5% bypass‡)	7

Complexities

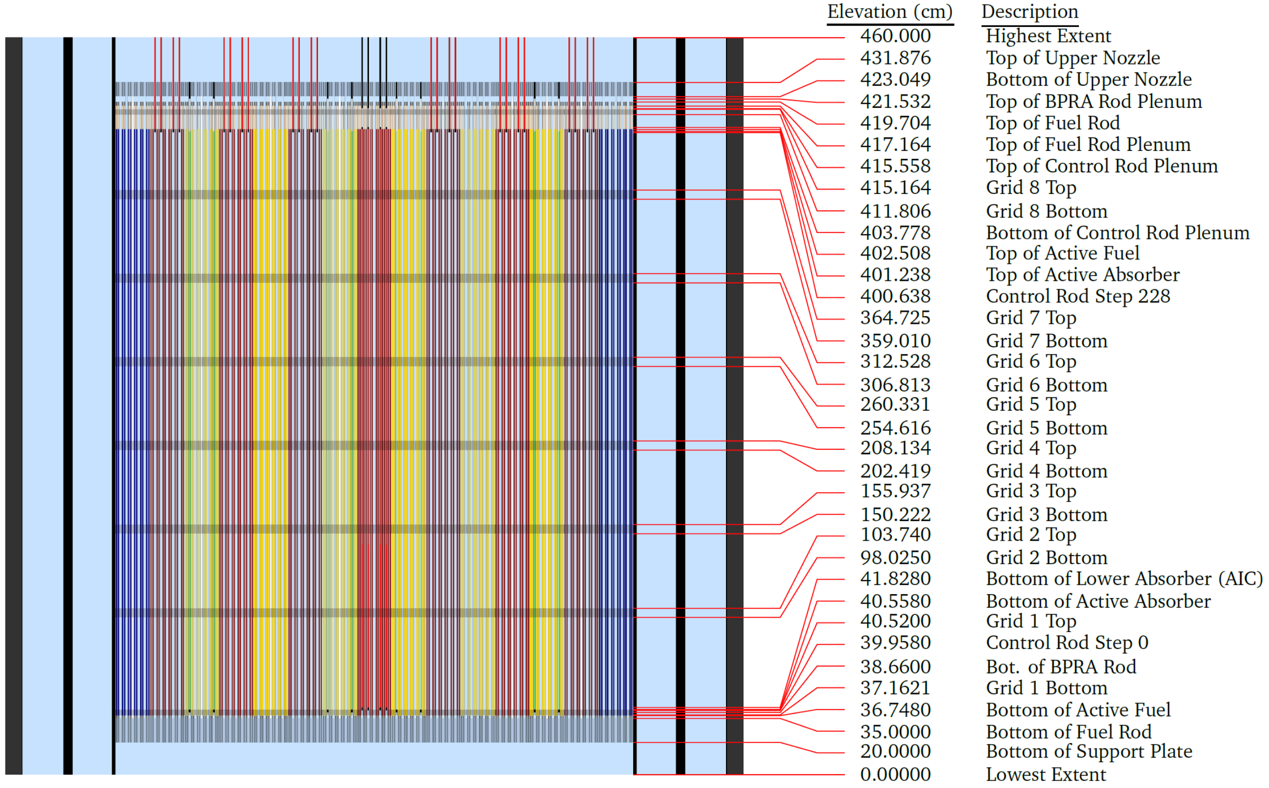

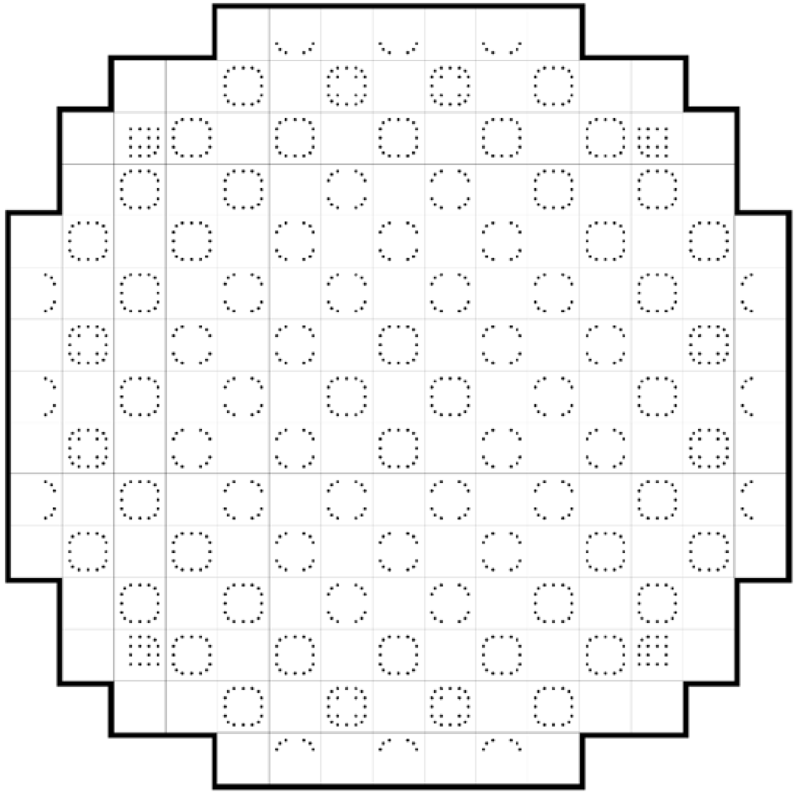

Figure 25: Detailed scale view of burnable absorber pins in cycle 1, showing proper rotations.

Measurements

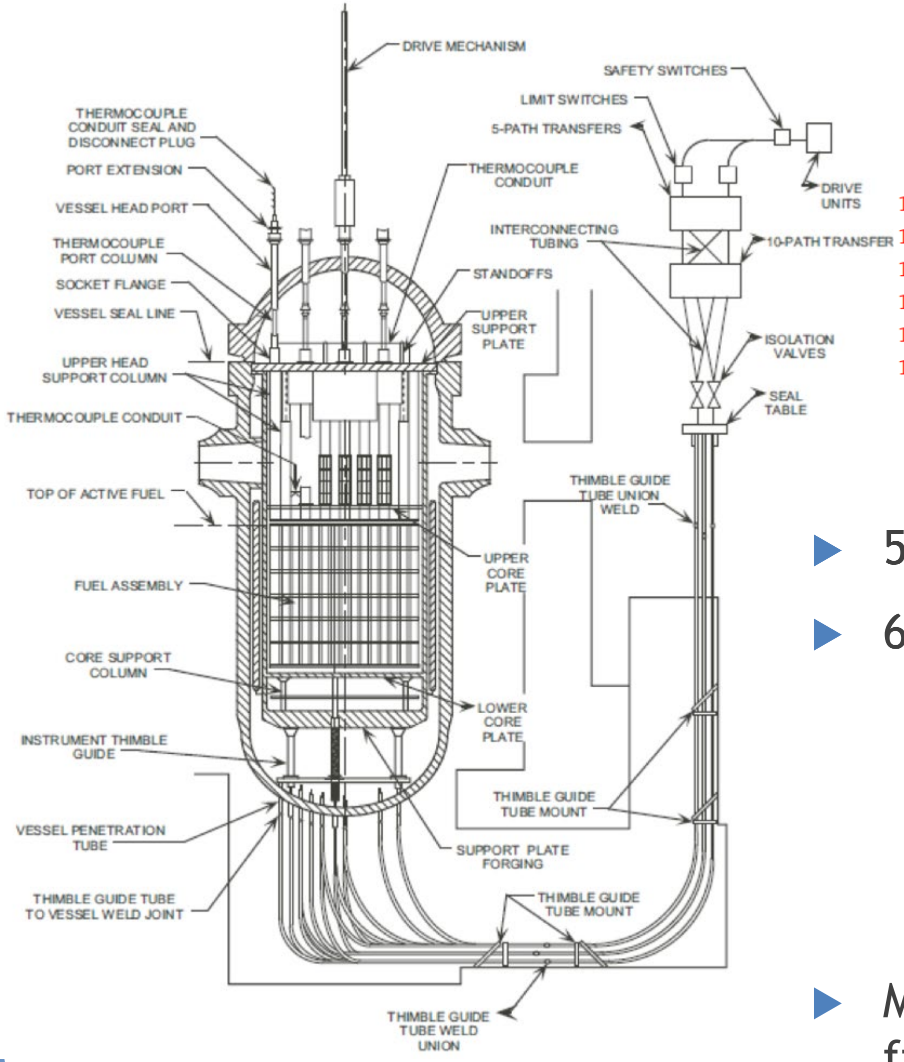

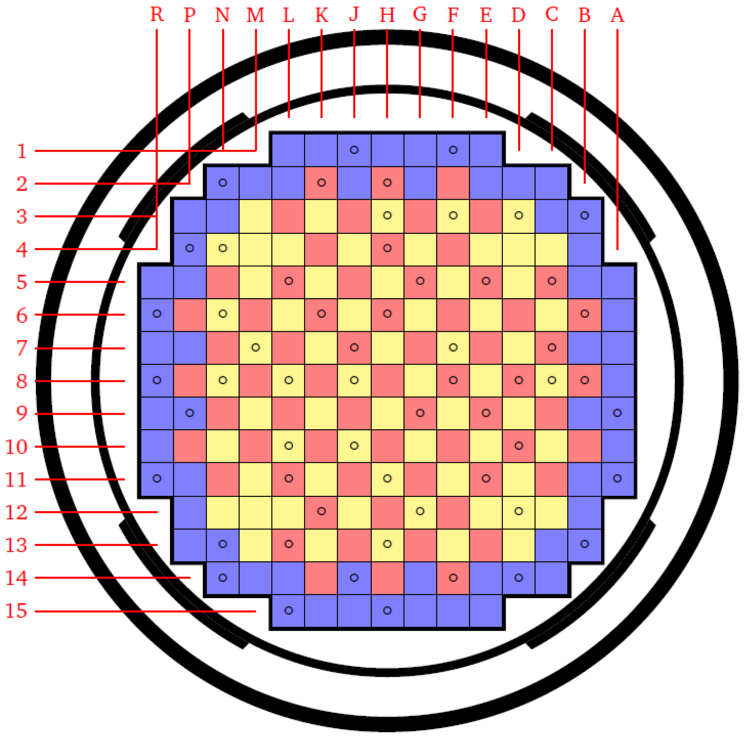

	H	G	F	E	D	C	B	A
8		0.774 — 1	1.065 0.032 2	0.943 0.036 2	1.145 0.042 2	0.937 0.045 4	1.259 0.051 2	0.784 0.076 2
9	0.774 — 1	1.013 0.006 2	0.920 — 1	1.152 0.033 2	0.924 — 1		0.919 — 1	0.845 — 1
10	1.065 0.032 2	0.892 — 1	1.101 — 1		1.257 0.048 2	0.942 0.032 2		0.685 0.020 2
11	0.943 0.036 2		0.964 — 1	1.251 0.068 4		1.339 — 1		0.616 0.020 2
12	1.145 0.042 2	1.034 — 1			1.438 — 1	1.143 0.039 2	0.875 — 1	
13	0.937 0.045 4	1.204 — 1		1.321 — 1		0.857 — 1	0.746 0.066 2	
14	1.259 0.051 2	0.837 — 1	1.256 0.094 3		1.050 — 1	0.667 0.031 2		
15	0.784 0.076 2	0.777 — 1		0.576 — 1				

- 58 assemblies that can be accessed by in-core detectors
- 6 fission chambers are used
  - One common location for normalization
  - Inserted from the bottom and pushed all the way to the top
  - Pulled back at constant speed with signal integrated over 61 axial positions
- Measurements are performed ~monthly with more testing during first cycle

Measurements

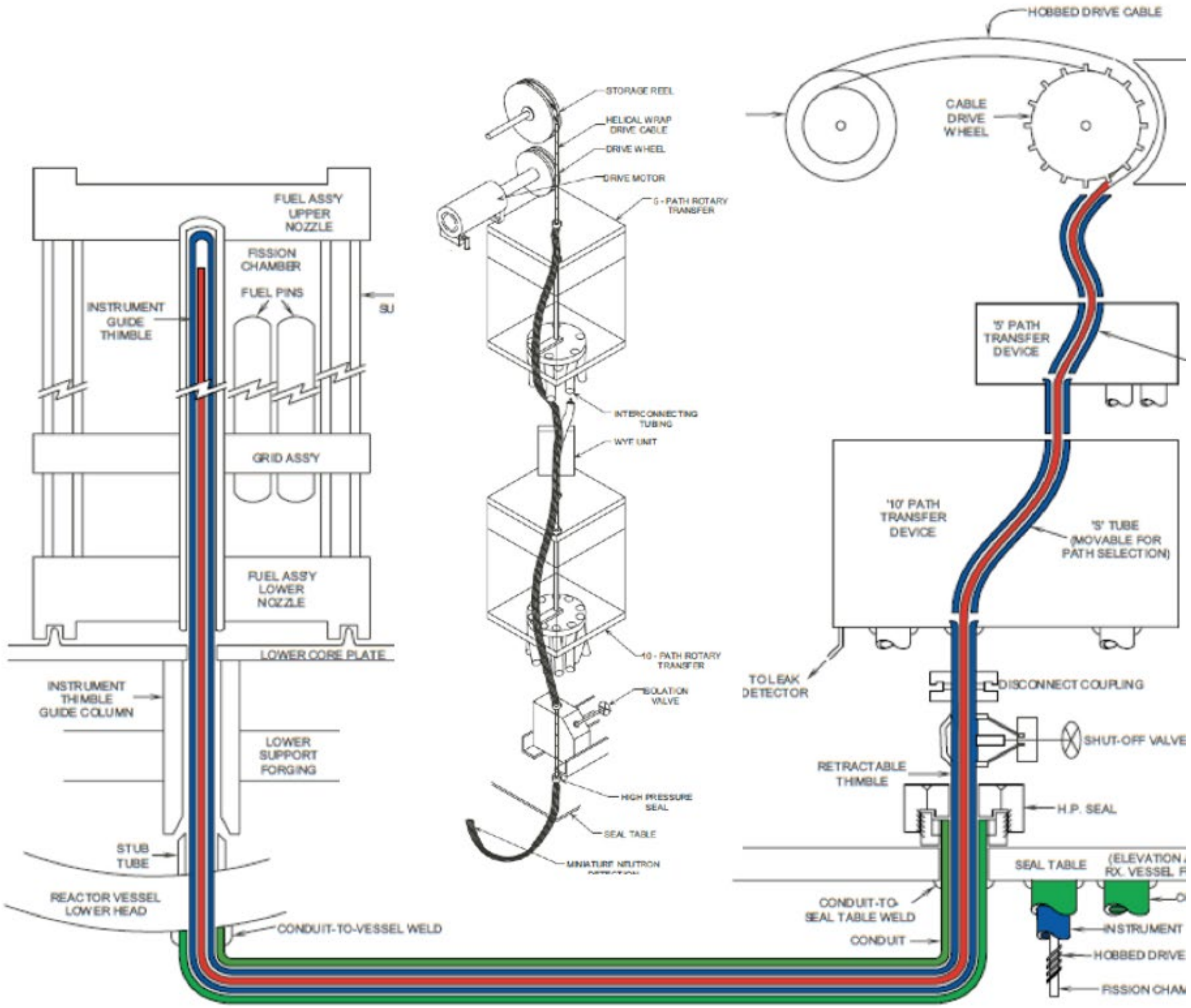

Figure 9.2-3 Movable Detector System

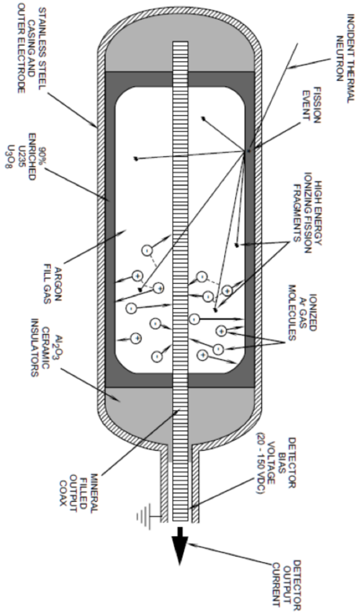

Post-Processing

- Normalized “flux”/detector signal obtained by removing the background (B) from the detector signal (D), multiplying by the gain (G) and dividing by core power

$$\phi_{ijk} = \frac{(D_{ijk} - B_{ij}) \times G_{ij}}{P}$$

- However, data is not directly usable
  - Misalignment of data
  - Missing data points
  - Data not continuous

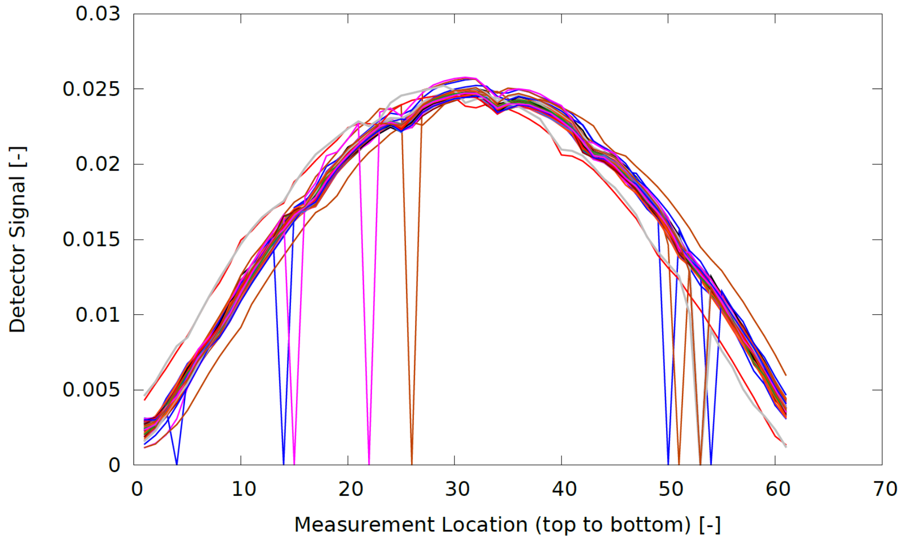

Figure 41: Initial Raw Detector Measurements (top to bottom).

S.KUMAR, J.LIANG, B.FORGET, K.SMITH “BEAVRS: An Integral Full Core Multi-Physics PWR Benchmark with Measurements and Uncertainties”, Progress in Nuclear Energy, 129, 2020.

Post-Processing

- Missing data points are removed through interpolation/extrapolation using nearest 2 neighbors
- Misalignment is corrected by assuming that grid depressions are all at the same axial level
- Second-order spline fit is performed to map axial data from top of active fuel to bottom of axial fuel

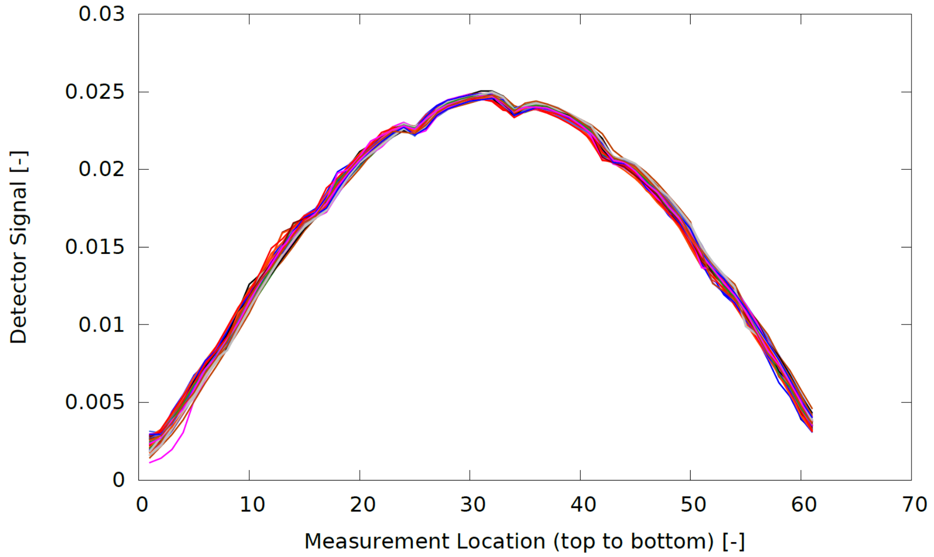

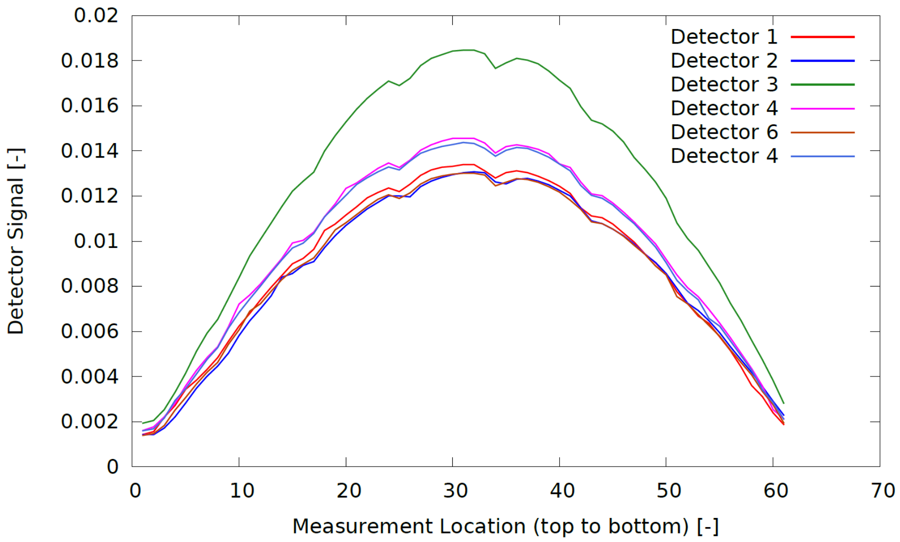

Uncertainties

$$\left(\frac{\delta_\phi}{\phi}\right)_m = \sqrt{\frac{\left(\frac{\partial\phi}{\partial D}\cdot\delta_d\right)^2+\left(\frac{\partial\phi}{\partial B}\cdot\delta_b\right)^2+\left(\frac{\partial\phi}{\partial G}\cdot\delta_g\right)^2+\left(\frac{\partial\phi}{\partial P}\cdot\delta_p\right)^2}{\phi^2}}$$

$$= \sqrt{\frac{\delta_d{}^2+\delta_b{}^2}{(D-B)^2}+\left(\frac{\delta_g}{G}\right)^2+\left(\frac{\delta_p}{P}\right)^2}$$

- Detector uncertainties were processed to include measurement and post-processing uncertainties.

$$\left(\frac{\delta_\phi}{\phi}\right)_{ijk} = \sqrt{\left(\frac{\delta_\phi}{\phi}\right)_m^2+\left(\frac{\delta_\phi}{\phi}\right)_{intp}^2+\left(\frac{\delta_\phi}{\phi}\right)_{align}^2+\left(\frac{\delta_\phi}{\phi}\right)_{spline}^2}$$

- Cycle 1 of BEAVRS includes 180 cases where multiple measurements were performed.
  - Cases of similar detector signal magnitude were grouped to provide better estimate of variance
  - 10,725 measurements were divided in 30 signal amplitude groups
- Missing data, re-alignment and spline fitting uncertainties were estimated by comparing measured data to interpolated data in case with known information, and by assuming possible misalignment by 1 axial position

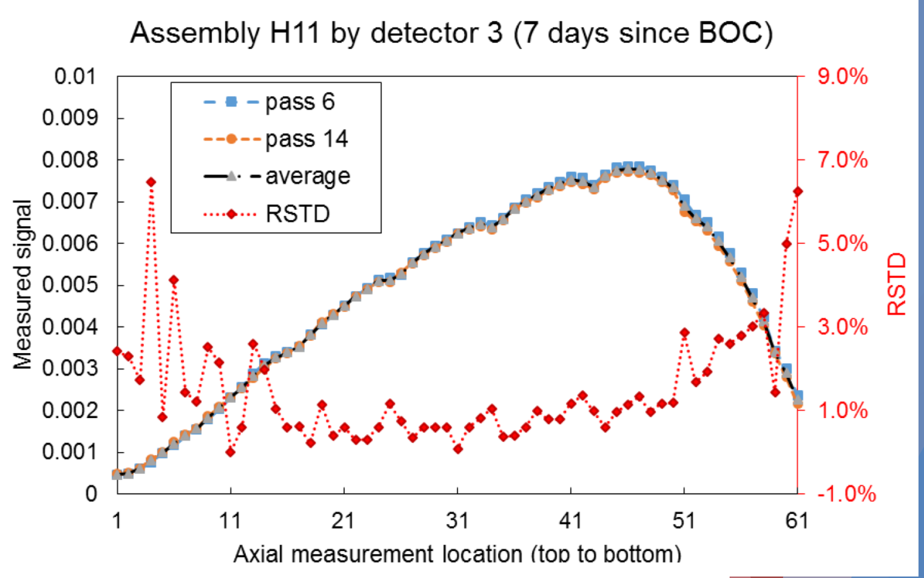

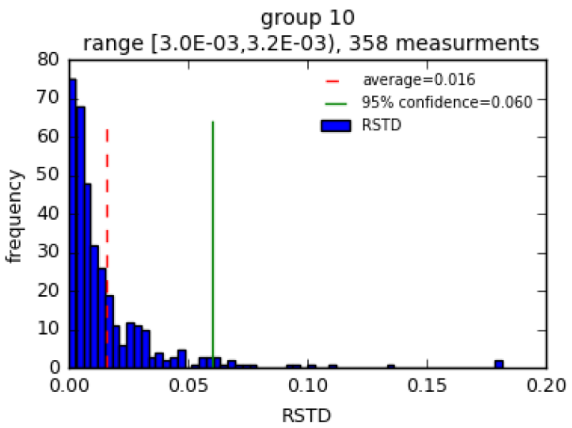

Uncertainties

- Lookup tables were generated using the repeated measurements and correction assessment such that uncertainty plots can be estimated for each measured assembly.
- Axially-integrated uncertainties were also calculated
- An independent approach was used based on simulation results to estimate axially-integrated uncertainties
  - Assumption is that deterministic code will predict short-term burnup trend well and that measurement fluctuations from prediction will be caused by measurement uncertainties

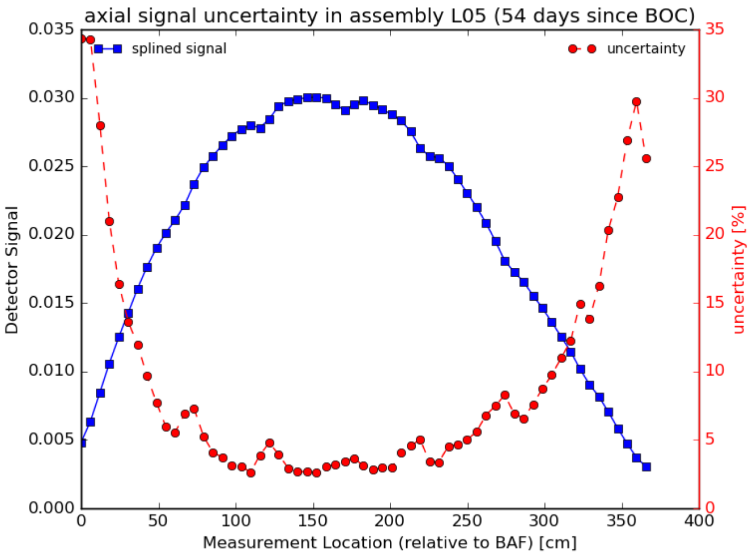

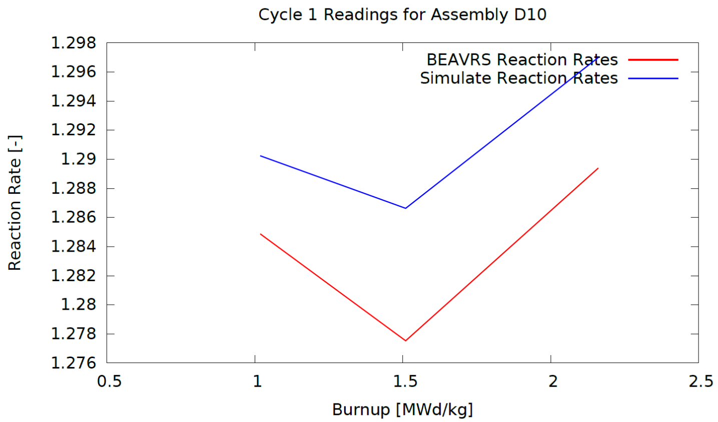

Fig. 17. Reaction rates for CASMO/Simulate and BEAVRS data for Assembly D10 at 1.02, 1.51, and 2.16 MWd/kg.

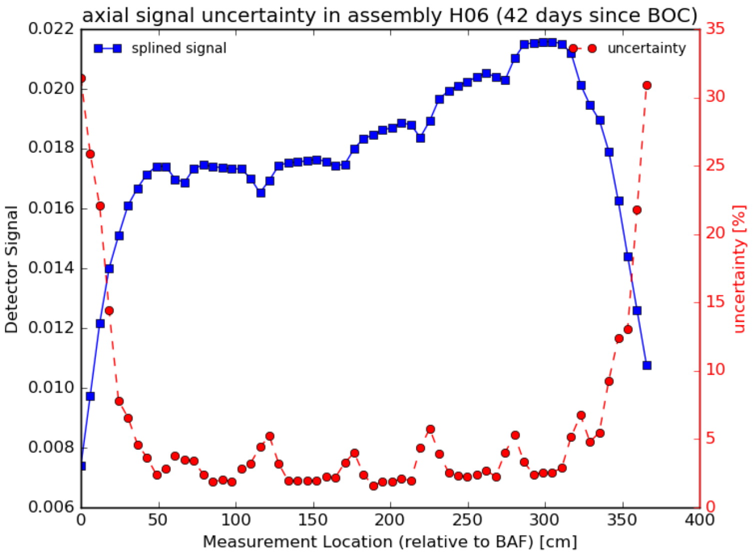

Liang, J., Kumar, S., Forget, B., Smith, K., 2017. Quantifying Uncertainty in the BEAVRS Benchmark, M&C 2017, Jeju, South Korea, 2017.

Uncertainties of Radial Map (95% CI)

- The measurement uncertainty (95% CI) is on the order of 1.5% regardless of the method used to assess the uncertainties.

	Method of Uncertainty Quantification		
	Multiple Measurements	Theoretical Analysis of Axial Uncertainties	Fitting Simulate Burnup Trends to BEAVRS data
Cycle 1	1.8%	1.4%	1.6%
Cycle 2	1.5%	1.4%	0.9%

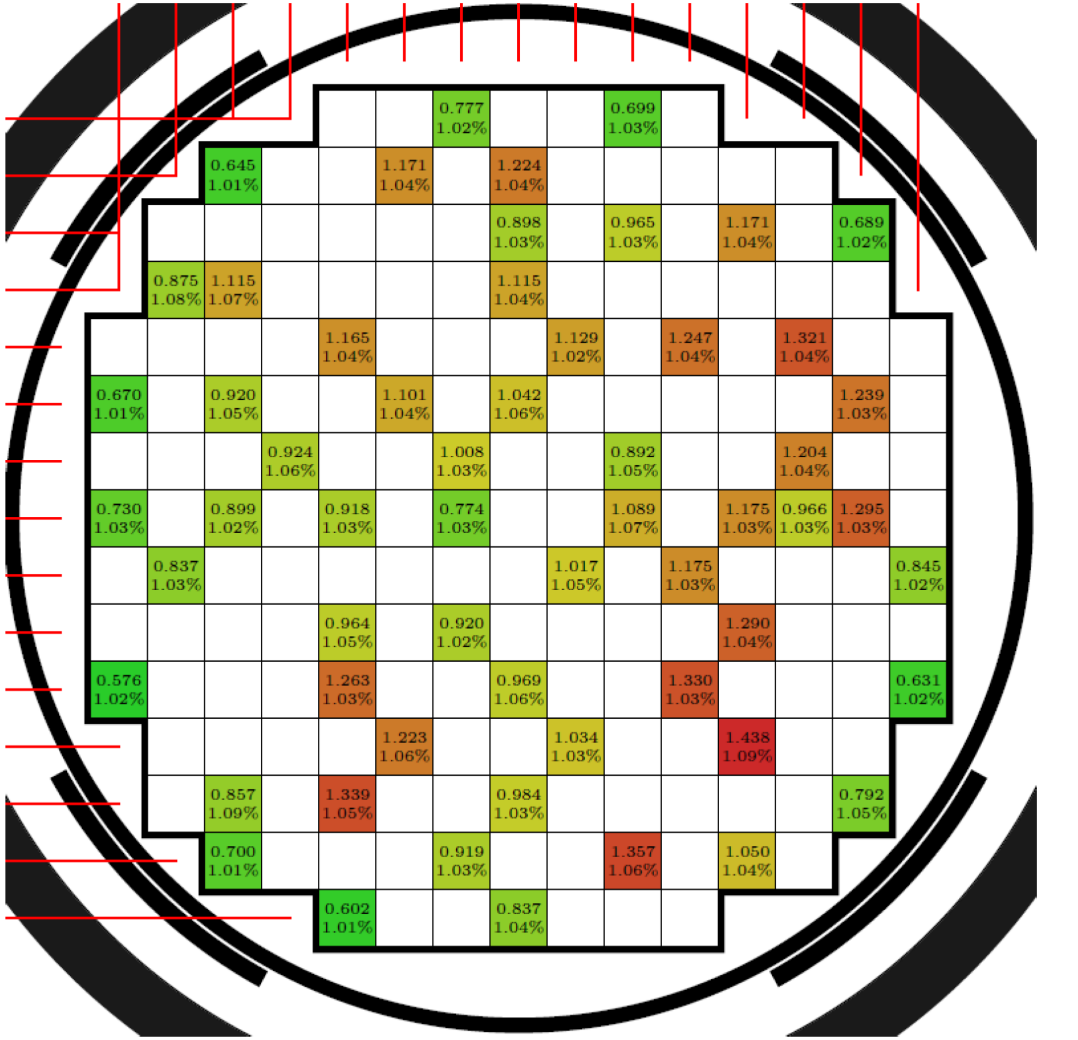

Issues

- Power History
- Tilt
- Inlet plenum mixing
- Material Compositions
- Missing as-built data
  - Gaps between assemblies/core loading
  - Boron isotopics
  - Data transcription errors
  - Grid spacer design
  - Upper and lower plate designs

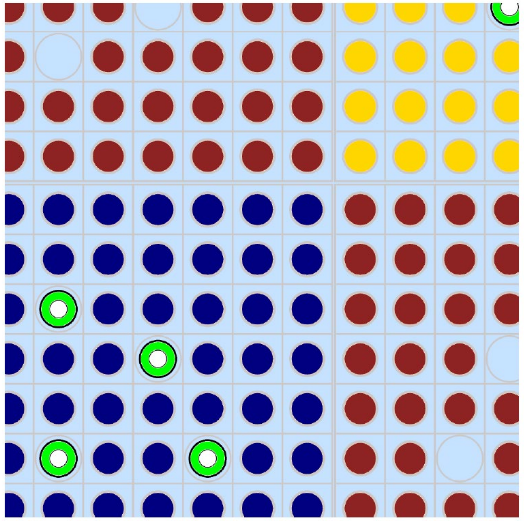

Grid Spacer was approximated as to converse height and mass

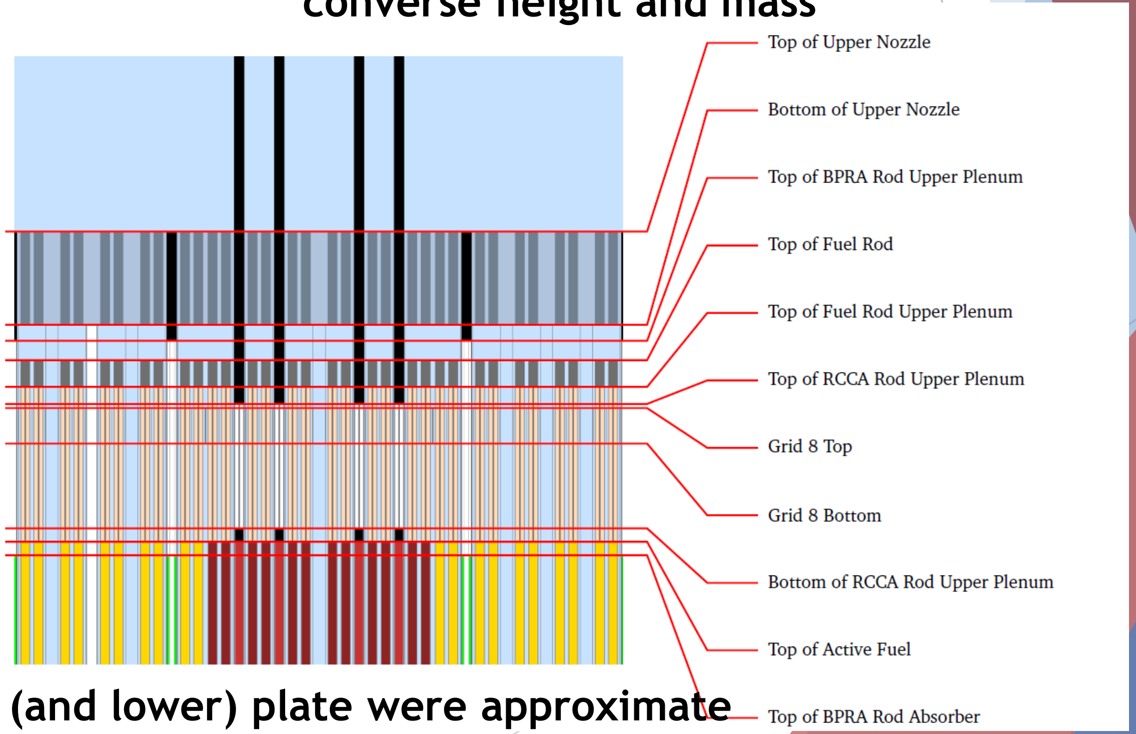

Upper (and lower) plate were approximate while leaving room for rods and water flow

Power History

- The power history of this reactor makes analysis very difficult due to the numerous shutdowns and power fluctuations
  - Many measurement points are taken when fission products have yet to reach an equilibrium
  - Some outliers have been identified when doing the time series analysis of cycle 1

Cycle 1 95% Confidence Interval of Errors		
Model	Model Fitting Uncertainty (with outliers)	Model Fitting Uncertainty (without outliers)
CASMO/SIMULATE	1.6%	0.8%
MPACT	1.6%	0.8%

Table 6
Cycle 1 95% CI of model fitting uncertainty with and without outliers at 1.02 and 9.80 MWd/kg using both CASMO/SIMULATE and MPACT.

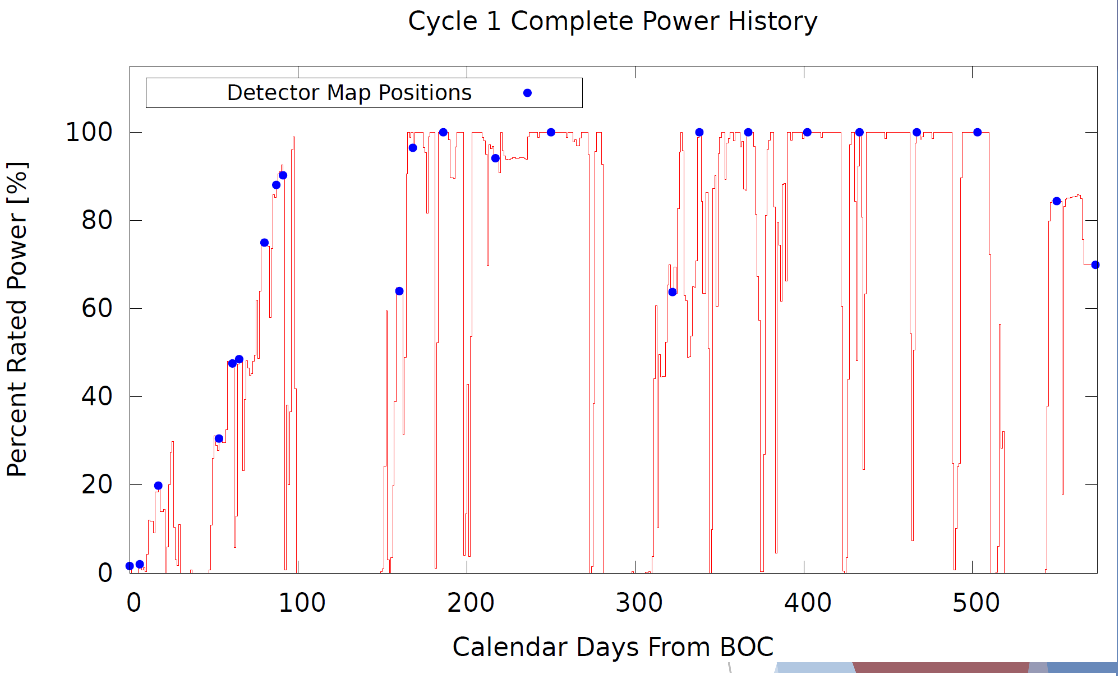

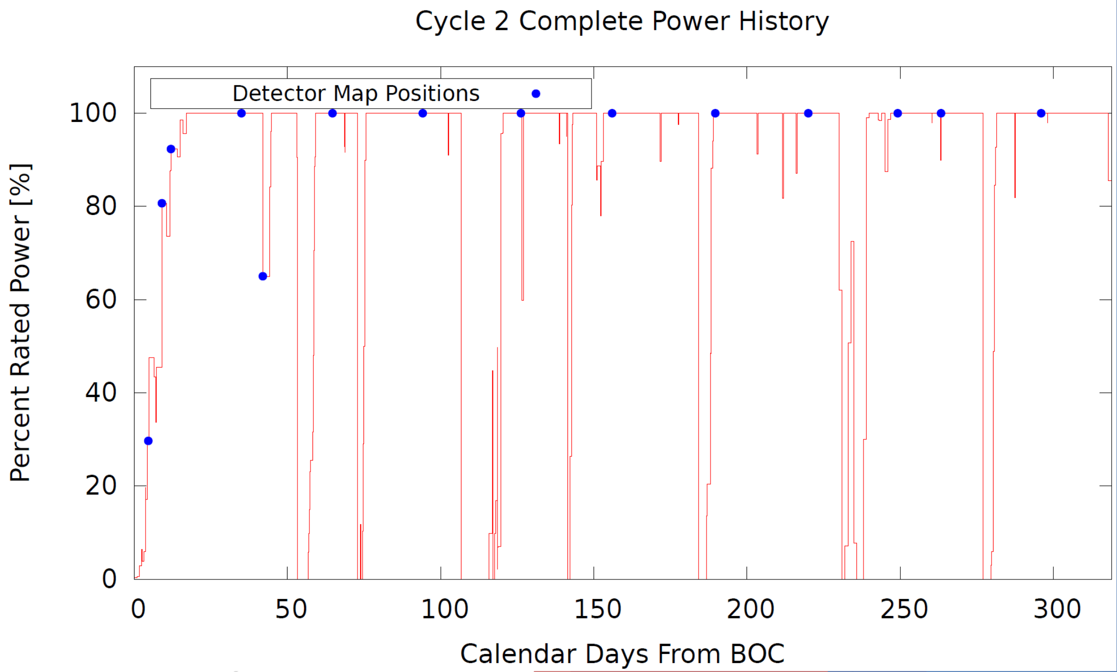

Tilt

Stanislas de Lambert Des Champs de Morel, "Contribution à l'analyse multiphysique de la déformation d'assemblage," Thèse Université Paris-Saclay, 2021

- Despite the core being fully-octant symmetric by design (with exception of instrument tubes), the measurements exhibit a large power tilt
- The cause of the tilt is largely unknown but suspected to be caused by uneven water gaps between assemblies during core loading
- Inlet plenum mixing is also a cause for concern, but generally doesn't lead to tilts of this magnitude on its own.

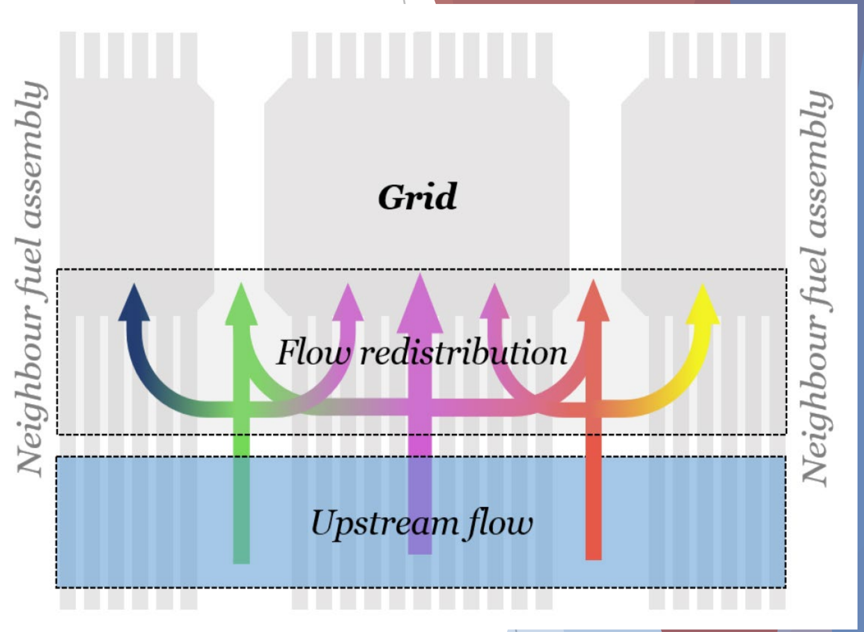

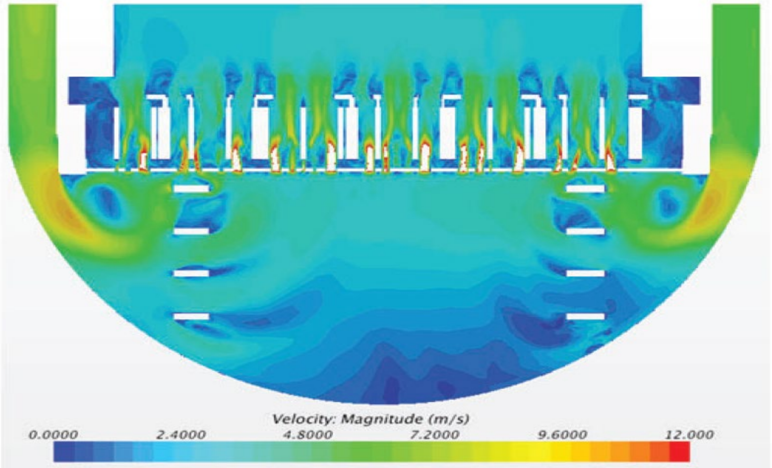

D.Y.Sheng, M.Seidl, "Towards the development of a full-scale transient CFD Model to simulate the static and dynamic in-core mass flux distribution in a classical German PWR, NURETH-16, Chicago, IL, 2015.

Tilt-Correction

- To make the data useful, a tilt-correction was proposed which identified a linear plane that would best correct the asymmetry of the data
  - This plane was then used to “correct” the detector signals for comparisons with high-fidelity codes
  - The linear tilt was also observed to decrease throughout operation, with the hypothesis being that thermal expansion evened out the gaps

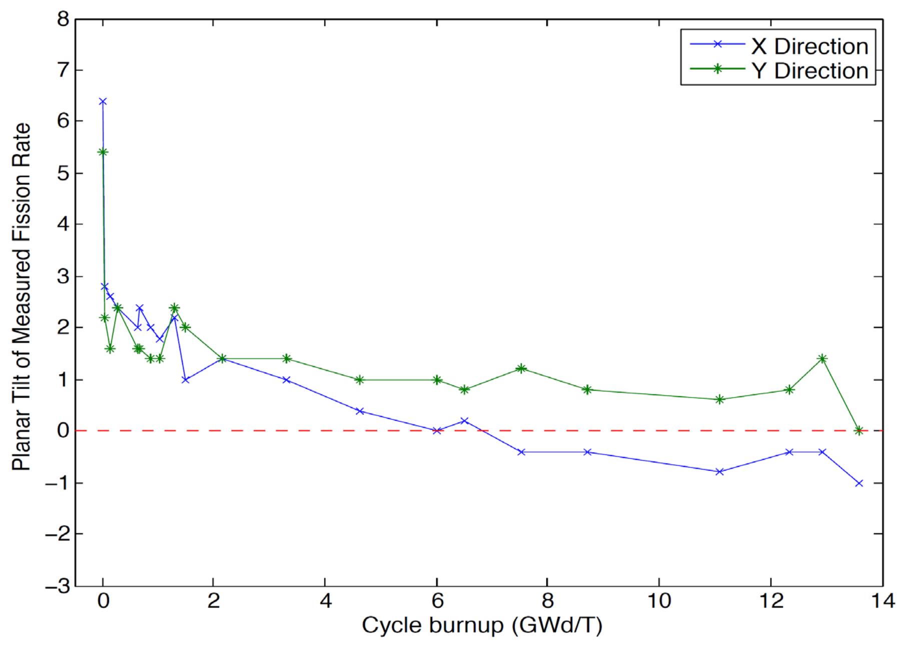

E. Sykora, “Testing the EPRI Reactivity Depletion Decrement Uncertainty Methods,” MIT MS Thesis, 2015

Tilt-Correction Impact on Uncertainty

- Brute force optimization approach was used to identify a water gap distribution in CASMO/SIMULATE that would best represent the measured data
- Linear tilt-correction is then applied to both the measured data and the tilted-model

Uncertainty Quantification Methods Based on CASMO/SIMULATE Model		
	CASMO/SIMULATE Model (before tilt-correction UQ)	CASMO/SIMULATE Model (after tilt-correction UQ)
Cycle 1	0.8%	1.8%
Cycle 2	0.9%	1.9%

Table 9
Summary of 95% CI of BEAVRS uncertainty quantification using CASMO/SIMULATE model.

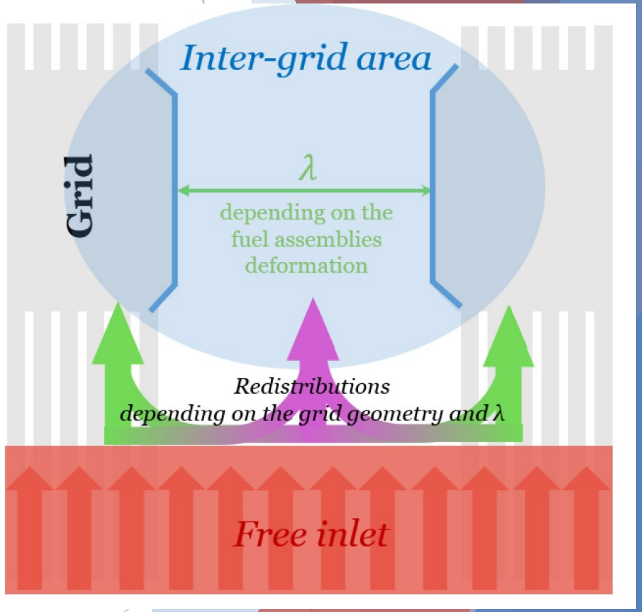

S.Kumar, Quantifying time-dependent uncertainty in the BEAVRS benchmark using time series analysis, MIT MS Thesis, 2018

Lessons Learned

- Real systems are very complex
  - While relatively simple, real systems have many complexities that can make them difficult to model with many modern tools
  - Even when trying to be rigorous and detailed, there is always missing design information
- Real systems are difficult to use for validation
  - There are many unknowns that cannot be easily measured of accounted for
  - They also lack the level of measurement precision
- Symmetric on paper is rarely symmetric in real life!

Monte Carlo Results

- Models have been developed for the following Monte Carlo codes:
  - OpenMC
  - MC21
  - Serpent
  - MCNP
  - JMCT
  - SuperMC
  - RMC
  - MVP
  - MCS
  - McCARD
  - …

Low Power Physics Tests – Rod Worths (pcm)

Rod Worth	Measured	OpenMC	MC21	JMCT	MVP	RMC	SuperMC	MCNP6	Serpent
D	788	771	773	770	787	798	779	775	785
C	1203	1234	1260	1258	1248	1233	1266	1250	1247
B	1171	1197	1172	1162	1230	1148	1180		1206
A	548	556	574	578	517	496	567	558	527
SE	461	501	544	543	473	475	532		488
SD	772	844	786	781	791	798	791		767
SC	1099	1049	1122	1107	1119	1137	1114	1110	1105
		-17	-15	-18	-1	10	-9	-13	-3
		31	57	55	45	30	63	47	44
		26	1	-9	59	-23	9		35
		8	26	30	-31	-52	19	10	-21
		40	83	82	12	14	71		27
		72	14	9	19	26	19		-5
		-50	23	8	20	38	15	11	6

Notes:
- Not all codes were run by their home institution
- These may not represent the latest results
- Most results are based on ENDF/B-7.1, but not all
- Everyone presents results slightly differently making them hard to compare

Run strategies

- There is a large variation in run strategies:
  - 4 million/batch, 1000 batches (400 discarded)
  - 4 million/generation, 50 generation/batch, 30,000 generations (250 discarded)
    - 120 billion active neutrons to achieve true variance below 1% on 95% of pellets
  - 1 million/batch, 750 batches (200 discard)
  - 500,000/batch, 200 batches (50 discard)
  - 500,000/batch, 350 batches (150 discard)
  - 200,000/batch, 400 batches (200 discard)
  - 10,000/sub-cycle, 300 sub-cycles/cycle, 44 cycles (4 discard)
  - … and some provide no information
  - … some also used acceleration techniques like CMFD to reduce discarded batches

Population Variance (1M/batch)

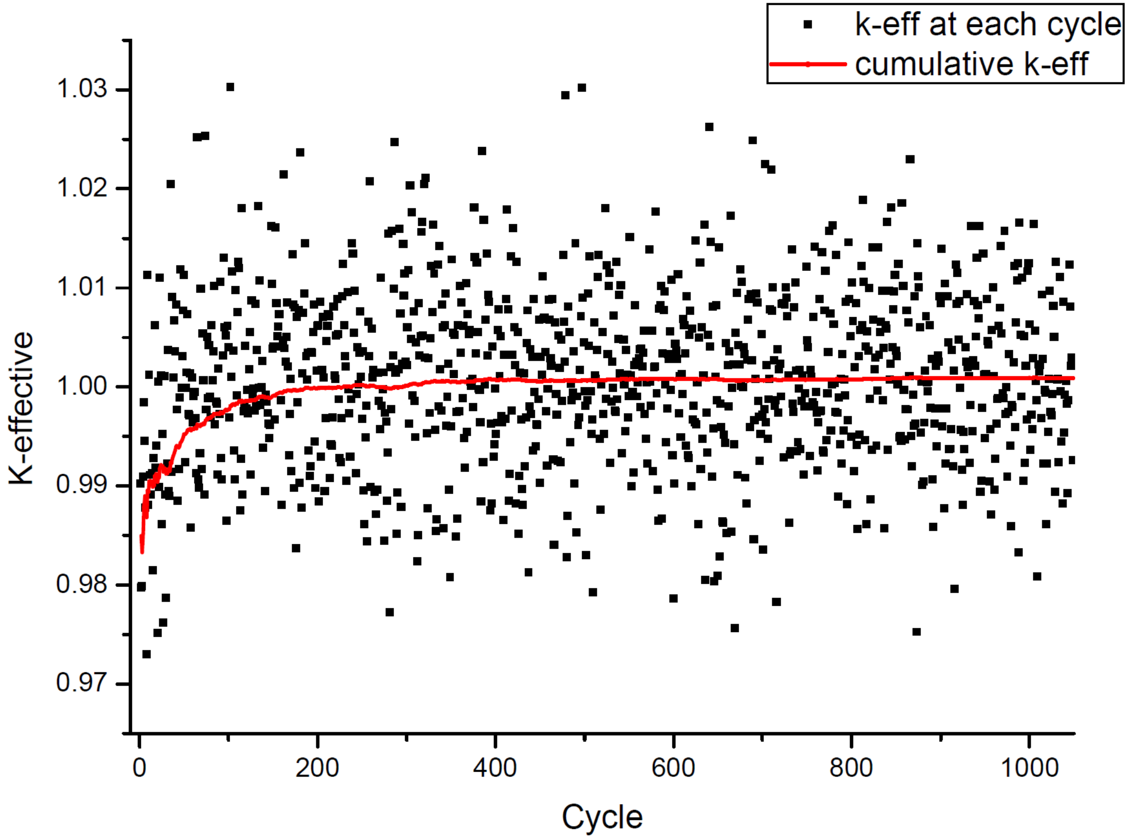

H.J.Park, H.C. Lee, J.Y. Cho, H.J. Shim, C.H. Kim, "Real Variance Estimation of BEAVRS Benchmark in McCARD Monte Carlo Eigenvalue Calculations", M&C 2015

- From CMFD, we determined that the dominance ratio of this core is on the order of 0.995.

Radial Distributions

- Results that rejected fewer than 100 batches exhibit discrepancies on the order of 2-3% from converged solutions
  - Massive in/out tilt
- Some simulations with very few particles per cycle/batch produced very distorted axial profiles
- Very few codes have attempted depletion over 2 cycles with TH coupling
  - Large tally cost
  - Convergence issues

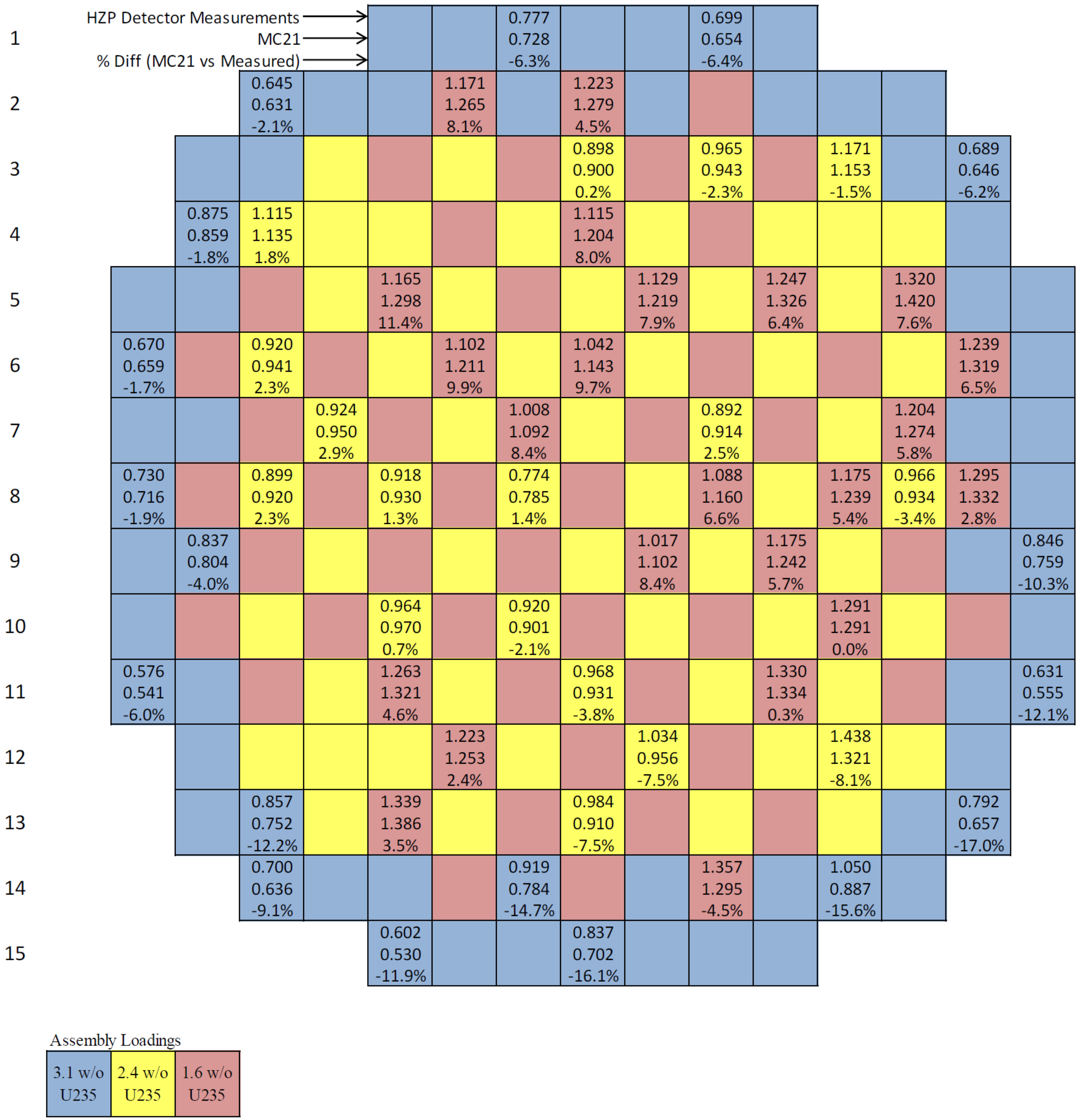

Source Convergence

- To properly understand source convergence, we developed a new diagnostics based on functional expansion tallies
  - Idea is that high order FETs will exhibit the noise of the system, and that the best possible convergence will be achieved when the lower order modes reach that same noise level.
  - Convergence differs based on the number of neutrons/batch
- Initial idea was developed based on discrete Fourier transforms that were post-processed from fine mesh tallies
- It was then extended to FETs since they can be directly tallied
- Convergence is determined based on moving averages over a given number of cycles compared to offset of previous batch of cycles

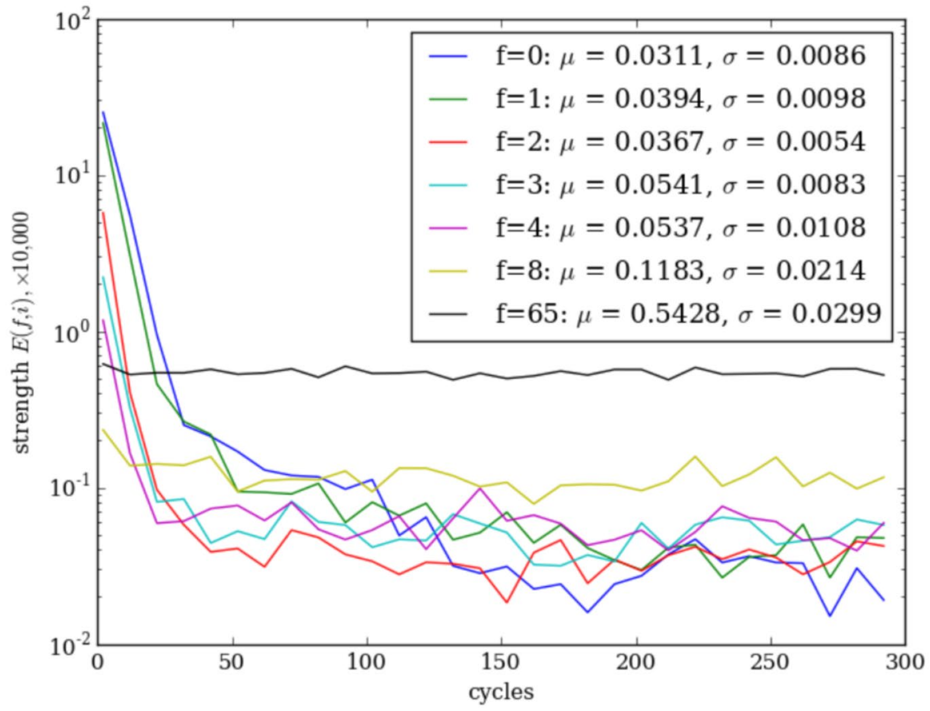

Discrete Fourier Transform of Radial 2D mesh

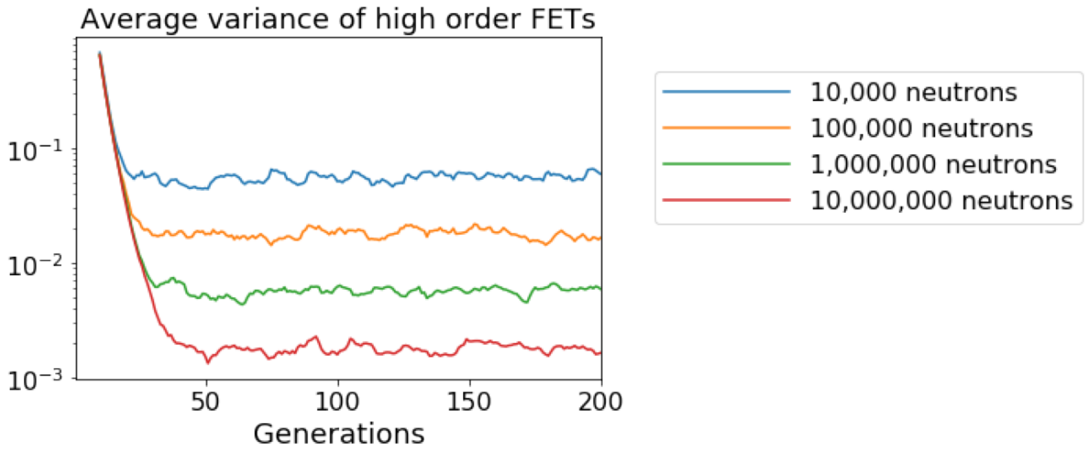

FET Estimate of Noise based on neutrons/cycles

- Luckily, the power predicted power profile of this core is quite flat such that a uniform guess of source sites is a great initial guess
  - FET and Shannon-based stationarity criteria indicate needing ~100 batches when using ~1M/batch
  - At this level, the modes have been reduced to the noise of the simulation
- However, the real problem is tilted from unknown geometrical irregularity, what would it take to converge this tilted problem?
  - Surrogate was developed by instead using a tilted source along y-axis
  - Under this scenario, ~600-800 batches must be discarded when using 10^5 to 10^7 neutrons/batch

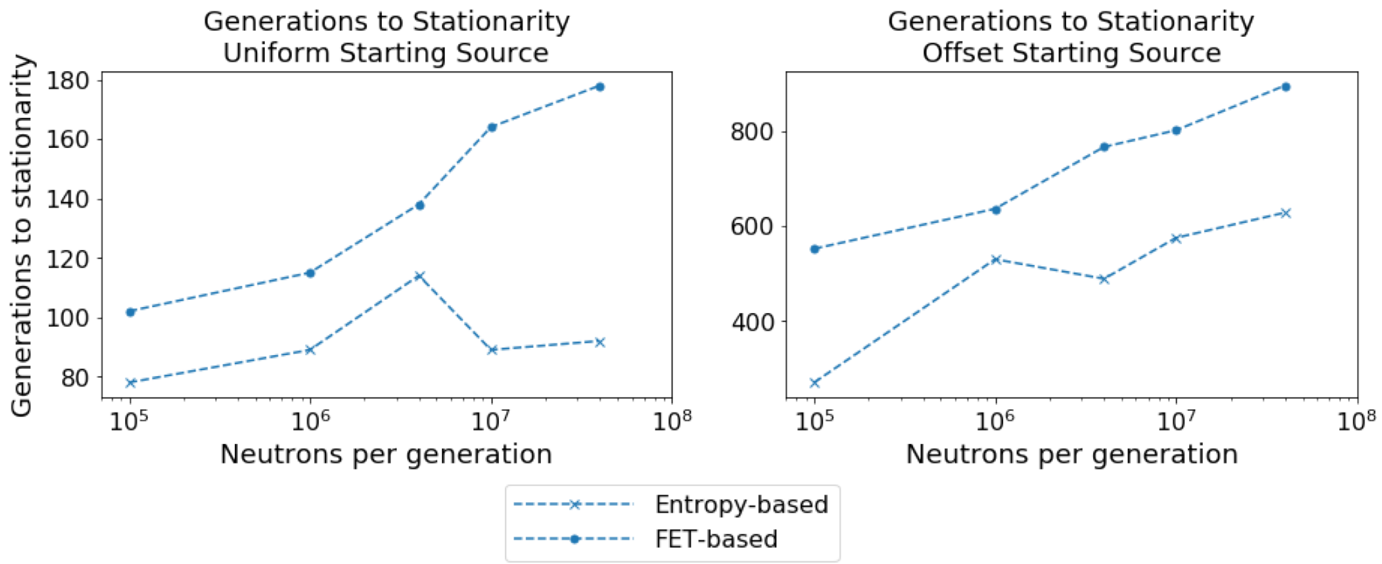

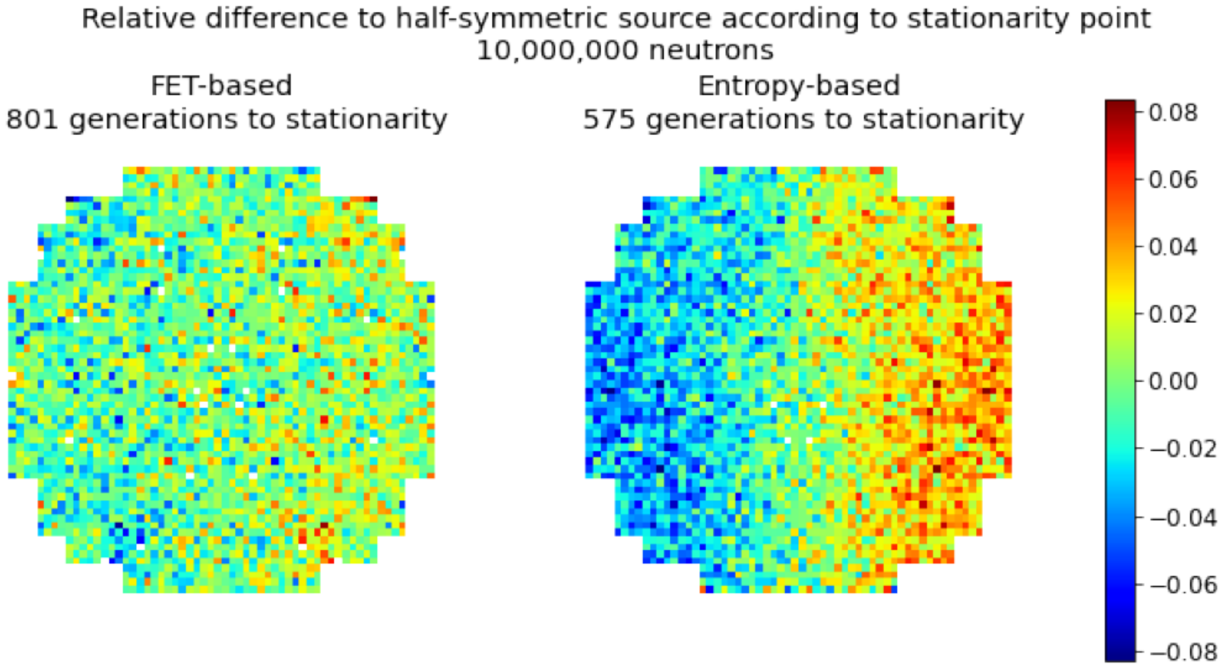

Impact of CMFD

- CMFD helps in the inactive cycles as can be seen in the FET coefficients
  - Reduced inactive cycles by x2 in example to the right
- However, CMFD is limited by the accuracy of its cross-section
  - If not sufficiently accumulated, it will increase observed variance

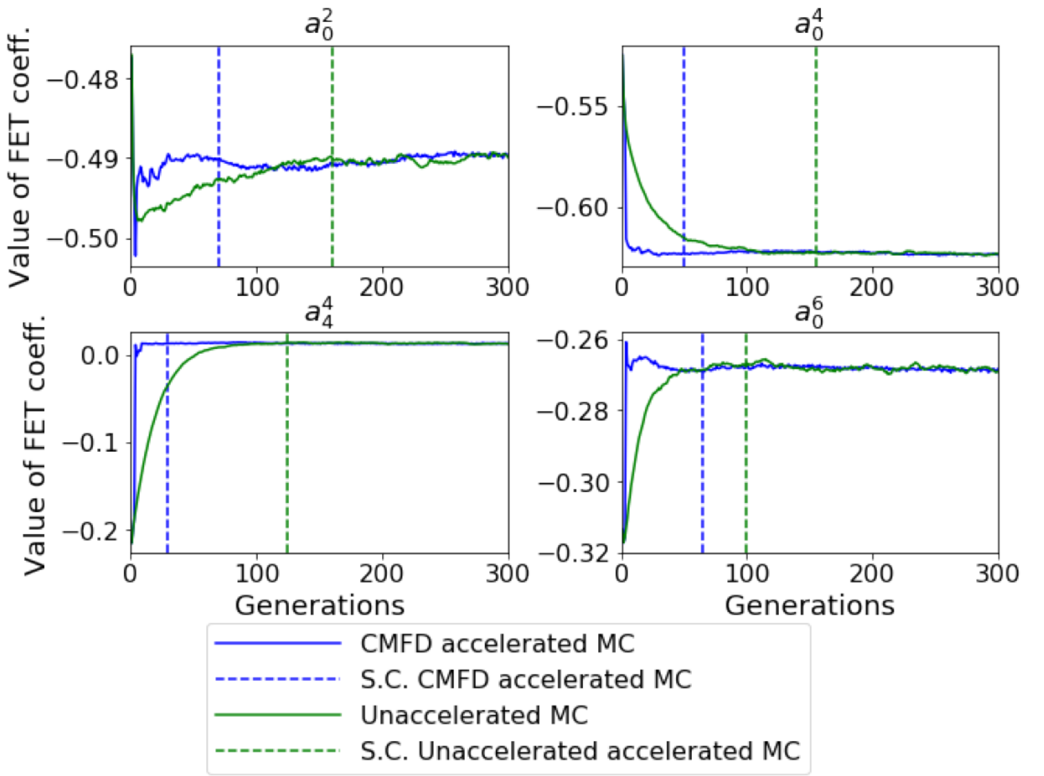

Figure 3-5: Value of representative FET coefficients as a function of generation number for the 2-D BEAVRS problem with CMFD acceleration (blue) and without CMFD acceleration (green). The dashed vertical lines represent the stopping criteria for each particular case.

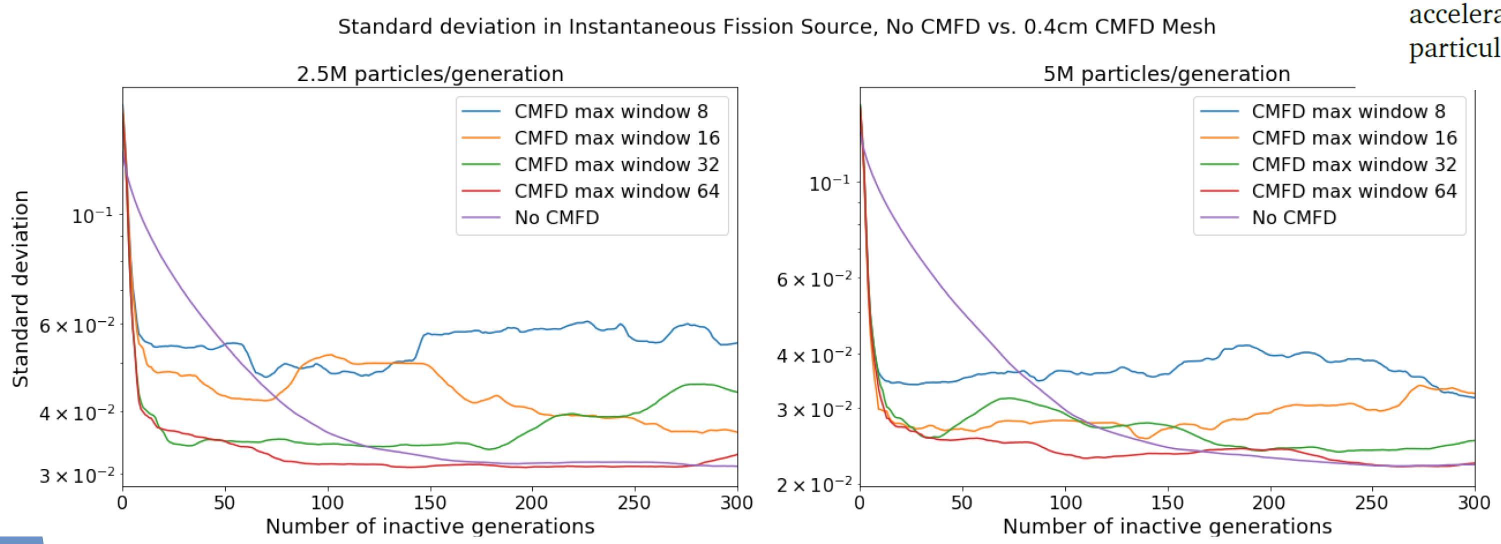

Deterministic Results

- BEAVRS benchmark was also used to demonstrate accuracy and efficiency of deterministic transport codes
  - Nodal Methods: SIMULATE, PARCS, PANTHER, PARAGON, KMACS, …
  - 2D/1D: nTracer, DeCART, MPACT, MAMMOTH, …
  - 3D MOC: OpenMOC (HZP only)
  - Deterministic codes demonstrated similar accuracy to MC
    - Also performed depletion over 2 cycles!
    - Performance is order of magnitude better
      - Seconds for nodal methods per state point
      - 10-100's hours for 2D/1D per state point
      - 1,000-10,000's hours for 3D MOC per state point
      - 10,000-100,000's hours for 3D MC per state point

Table 4. Comparison of BOC1 HZP control rod worth with measurements and OpenMC.

Case	Measured pcm	CRW nTRACER	CRW OpenMC†
D	788	776 (−12)*	771 (−17)
C with D in	1203	1210 (7)	1234 (31)
B with D, C in	1171	1230 (59)	1197 (26)
A with D, C, B in	548	535 (−13)	556 (8)
SE with D, C, B, A in	471	455 (−16)	501 (30)

*Numbers within the parenthesis are the difference from the measured value in pcm.
†The standard deviation of the OpenMC cases is about 5 pcm.

Table 6
Comparison of control rod bank worth by various reactor physics code calculations.

Case	Difference of CRBW (%)[a]				
	DeCART	VERA [6]	nTRACER [7]	PARCS [8]	McCARD
D with ARO	0.5	2.0	1.5	3.3	4.2
C with D in	−4.4	−3.5	−0.6	4.5	0.6
B with D, C in	−7.2	−0.8	−5.0	−11.3	4.7
A with D,C,B in	7.3	−3.5	2.4	31.8	−0.3
SE with D,C,B,A in	0.8	2.1	3.4	27.4	−11.1
Total	−2.4	−1.3	−0.8	5.8	0.7

[a] Difference of CRBW (%) = {CRBW(Measurement) − CRBW(DeCART)}/{CRBW(Measurement)} × 10^2.

Issues in modelling

- Complexity!
  - Lots of cells and surfaces – broke initial OpenMC XML reader
- Costly for Monte Carlo (and 3D transport)
  - Lots of particles needed, lots of cycles to model non-symmetric system
  - Lots of storage needed for reaction rates and nuclides
  - Convergence is costly
- Removal of Pyrex
  - Burnable absorbers must be removed from guide tubes after cycle 1, before shuffling into cycle 2
- Thermal expansion in high-fidelity codes
  - The use of lattices and replication makes it hard to capture thermal expansion or every region
  - Nodal methods capture this easily during lattice calculations
- Fuel shuffling

Final Remarks on BEAVRS Benchmark

- There is a need for large scale realistic benchmark for validation
  - They challenge the community is developing codes and methods focused on the real applications.
  - It identifies gaps and limitations of codes and run strategies.
- The BEAVRS benchmark however is limited in its usefulness
  - Power history is very jagged making it difficult to assume an equilibrium of fission products.
  - Tilt is quite large, leading to large uncertainties in measurements.
- **Newer data is needed that includes good power history, detailed measurements, redundant cores, …**
  - New construction sites have many replicas of exact first cycle core loads
  - Updated core instrumentation logs 610 axial measurements

Acknowledgements

- MIT
  - Bryan Herman, Nicholas Horelik, Matt Ellis, Jingang Liang, Shikhar Kumar, Paul Romano, Koroush Shirvan, Kord Smith, Benoit Forget
- Review
  - NNL – KAPL
    - Dan Kelly, Brian Aviles
  - ORNL – CASL
    - Ben Collins, Andrew Godfrey
- Funding
  - DOE NEUP, CASL, CESAR

PART II: Analytical Benchmark

Analytical Benchmark

- What is it?
  - Goal was to derive an analytical benchmark of the transport equation to validate our uncertainty quantification methods
    - Provides forward and adjoint solution
    - Additionally, it provides validation of continuous energy Monte Carlo

NUCLEAR SCIENCE AND ENGINEERING · VOLUME 195 · 795–812 · AUGUST 2021

DOI: https://doi.org/10.1080/00295639.2021.1874777

ANS

An Analytic Benchmark for Neutron Boltzmann Transport with Downscattering—Part I: Flux and Eigenvalue Solutions

Vladimir Sobes,[a]* Pablo Ducru,[b] Abdulla Alhajri,[b] Barry Ganapol,[c] and Benoit Forget[b]

[a]*University of Tennessee, 1412 Circle Drive, Knoxville, Tennessee 37996*
[b]*Massachusetts Institute of Technology, 77 Massachusetts Avenue, Cambridge, Massachusetts 02139*
[c]*The University of Arizona, 1130 North Mountain Avenue, Tucson, Arizona 85721*

Received October 1, 2020
Accepted for Publication January 7, 2021

$$
\left[\frac{1}{v}\frac{\partial}{\partial t} + \Omega \cdot \nabla + \Sigma_t(E)\right]\phi(r,\Omega,E,t)
$$

$$
= \int_{E_0}^{E_\infty} dE' \int_{4\pi} d\Omega' \Sigma_s(\Omega' \to \Omega, E' \to E)\phi(r,\Omega',E',t)
$$

$$
+ \frac{\chi(E)}{4\pi}\int_{E_0}^{E_\infty} dE' \int_{4\pi} d\Omega' \nu(E')\Sigma_f(E')\phi(r,\Omega',E',t) + Q(E)
$$

Assumptions

- Infinite Medium
- Scattering isotope of mass 1 (no Plazcek transients)
- No upscattering
- Steady-state (alpha = 0) and exactly critical (k=1)
- **Energy independent fission spectrum**
- No external sources

$$\Sigma_t(E)\psi(E) = \int_E^{E_\infty} dE' \frac{\Sigma_s}{E'}\psi(E') + \chi(E)\int_{E_0}^{E_\infty} dE' \nu\Sigma_f(E')\psi(E')$$

Solution

- A few definitions

$$D_S{}^{\alpha}(E) \triangleq \frac{\Sigma_s(E)}{E\Sigma_t^{\alpha}(E)} \qquad f_\nu^{\alpha}(E) \triangleq \frac{\nu\Sigma_f(E)}{\Sigma_t^{\alpha}(E)} \qquad R_\alpha(E) \triangleq \Sigma_t^{\alpha}(E)\,\psi_\alpha(E) \qquad F_\alpha \triangleq \int_0^{E_\infty} f_\nu^{\alpha} R_\alpha dE$$

- Total reaction rate (alpha-mode)

$$R_\alpha(E) = F_\alpha\left[\chi(E) + \int_E^{E_\infty} \chi(E')D_S{}^{\alpha}(E')e^{\int_E^{E'} D_S{}^{\alpha} dE''} dE'\right]$$

- In k-mode

$$k = \int_0^{E_\infty} f_\nu(E)\left[\chi(E) + \int_E^{E_\infty} \chi(E')D_S(E')\, e^{\int_E^{E'} D_S} dE'\right] dE$$

$$R_k(E) = \frac{F_k}{k}\int_{E_\infty^+}^{E} \frac{d\chi}{dE}(E')\, e^{\int_E^{E'} D_S} dE'$$
$$= \frac{F_k}{k}\left[\chi(E) + \int_E^{E_\infty} \chi(E')D_S(E')\, e^{\int_E^{E'} D_S} dE'\right]$$

Special case – Step fission spectrum

- By simplifying the fission spectrum and defining the cross-sections using a pole/residue representation

$$\chi(E) \triangleq \chi_0 1[E < E_\infty]$$

$$D_S{}^{\alpha}(x) = \sum_{n=1}^{N_p} \frac{a_n}{x - b_n}$$

- We can obtain analytical solutions for all of our quantities of interest

$$R_\alpha(E) = \chi_0 F_\alpha \prod_{n=1}^{N_p} \left(\frac{\sqrt{E_\infty} - b_n}{\sqrt{E} - b_n} \right)^{a_n}$$

A simple benchmark

Quantitative Description of the Benchmark Inputs

Material	Fission Isotope	Capture Isotope	Scattering Isotope
Description	Lowest lying resonance of ^{239}Pu	Lowest lying s-wave resonance of ^{238}U	Flat scattering cross section
N	1.00	0.124954	0.008340505
ν	2.88	0	0
g_J	3/4	1	
E_λ (eV)	2.956243e-1	6.674280e+0	
Γ_n (eV)	7.947046e-5	1.492300e-3	
Γ_γ (eV)	3.982423e-2	2.271100e-2	
Γ_f (eV)	5.619673e-2	9.880000e-9	
a_c (10^{-12} cm)	9.410000e-4	9.480000e-4	
σ_s (b)			20.0
ρ_0	0.002196807122623 $\times$ 1/2	0.002196807122623 $\times$ 1/2	0.002196807122623 $\times$ 1/2

- Picked data such that k = 1
- 2 resonances and a scatterer (H-1)

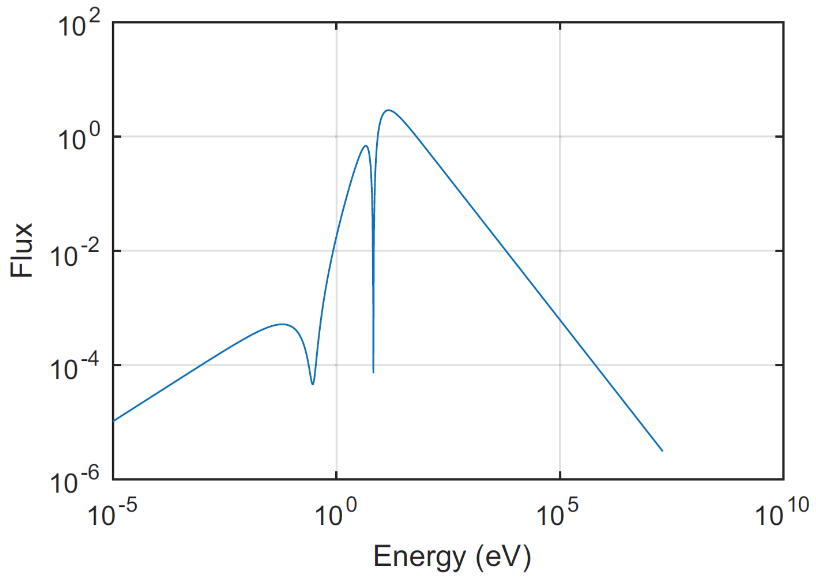

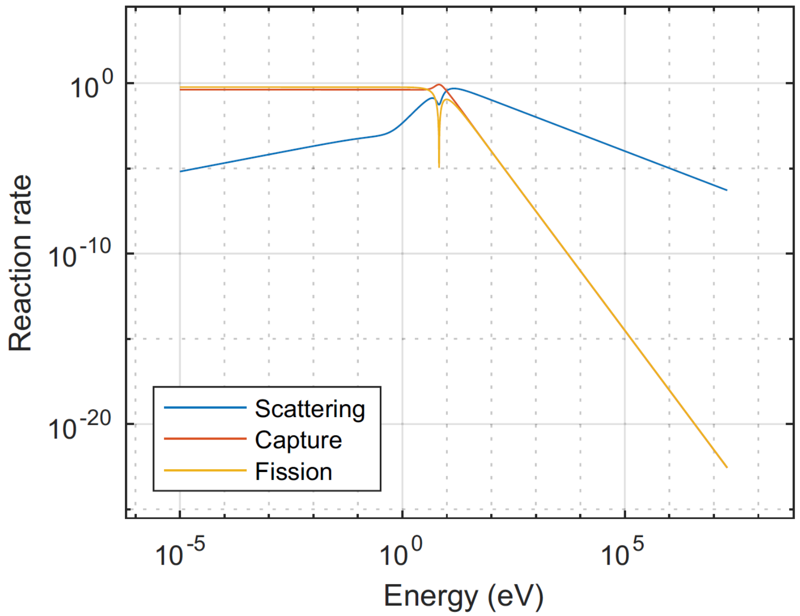

Extension to UQ

$$\psi_0^\dagger = \frac{1 - \int_{E_0}^{E_\infty} D_S(E) \prod \left(\sqrt{E} - b_n\right)^{a_n} \left(\int_{E_0}^{E} F_{S'}(E') \prod \left(\sqrt{E'} - b_n\right)^{-a_n} dE' \right) dE}{\frac{1}{D_S(E_0)} \left[\prod \left(\frac{\sqrt{E_\infty} - b_n}{\sqrt{E_0} - b_n} \right)^{a_n} - 1 \right]}$$

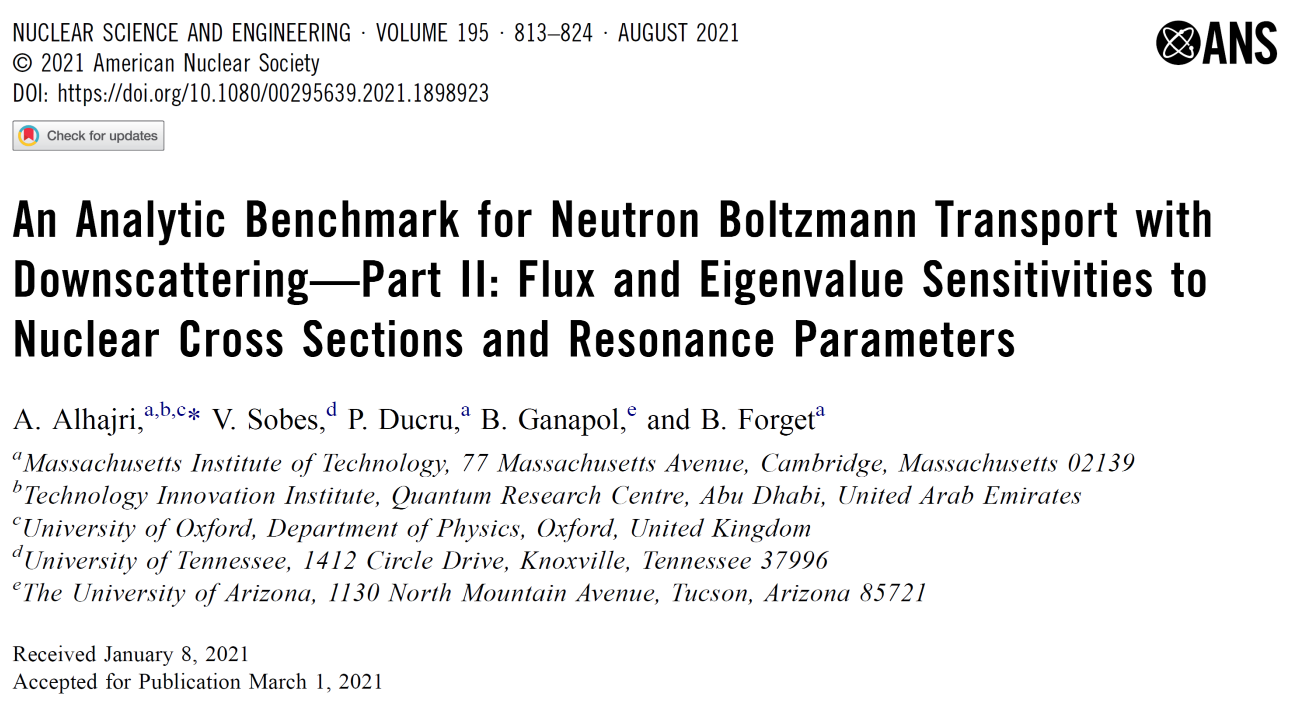
NUCLEAR SCIENCE AND ENGINEERING · VOLUME 195 · 813–824 · AUGUST 2021

DOI: https://doi.org/10.1080/00295639.2021.1898923

ANS

An Analytic Benchmark for Neutron Boltzmann Transport with Downscattering—Part II: Flux and Eigenvalue Sensitivities to Nuclear Cross Sections and Resonance Parameters

A. Alhajri,[a,b,c]* V. Sobes,[d] P. Ducru,[a] B. Ganapol,[e] and B. Forget[a]

[a]*Massachusetts Institute of Technology, 77 Massachusetts Avenue, Cambridge, Massachusetts 02139*
[b]*Technology Innovation Institute, Quantum Research Centre, Abu Dhabi, United Arab Emirates*
[c]*University of Oxford, Department of Physics, Oxford, United Kingdom*
[d]*University of Tennessee, 1412 Circle Drive, Knoxville, Tennessee 37996*
[e]*The University of Arizona, 1130 North Mountain Avenue, Tucson, Arizona 85721*

Received January 8, 2021
Accepted for Publication March 1, 2021